Applied Science and Engineering Progress, Vol. 20, No. 3, 2027, 8259

Research Article

Sustainable Valorization of *Phragmites australis* and *Cyperus papyrus* Phytoremediation Biomass into Biochar for Methylene Blue Removal

Keneilwe Motlakatlala* and Stephen Majoni
Department of Chemical and Forensic Sciences, School of Pure and Applied Sciences, Botswana International University of Science and Technology, Palapye, Botswana

Venecio U. Ultra
Department of Sustainable Mineral Resources, School of Earth Sciences and Engineering, Botswana International University of Science and Technology, Palapye, Botswana

Phillip Oladijo
Department of Chemical, Material and Metallurgical Engineering, School of Earth Sciences and Engineering, Botswana International University of Science and Technology, Palapye, Botswana

* Corresponding author. E-mail: mk18000975@biust.ac.bw DOI: 10.14416/j.asep.2026.08.010
Received: 30 March 2026; Revised: 2 June 2026; Accepted: 15 June 2026; Published online: 19 August 2026

Abstract
Mining activities at the copper nickel Bamangwato Concessions Limited (BCL) mine have contributed to the accumulation of heavy metals in areas surrounding the mining town. Although phytoremediation plants naturally help remediate contaminated soils, they generate large amounts of biomass that require sustainable management. This study explored the use of biochar obtained from phytoremediation biomass of *Cyperus papyrus* (CP) and *Phragmites australis* (PA) collected from the BCL mine site for the adsorption of Methylene Blue from aqueous solutions as a sustainable strategy for managing phytoremediation waste. The effects of several parameters, including contact time, adsorbent dosage, temperature, and initial dye concentration, on the adsorption process were investigated. The results showed that adsorption efficiency for both biochars had a positive correlation with contact time, higher initial dye concentration, increased adsorbent dosage, and solution pH. To better understand the adsorption mechanism, kinetic and thermodynamic analyses were conducted. The adsorption behavior was best described by the Langmuir isotherm model and the Elovich kinetic model. The maximum adsorption capacities were determined to be 128.21 mg/g for CP biochar and 79.35 mg/g for PA biochar. The results demonstrate that biochar produced from phytoremediation biomass of CP and PA can effectively remove organic contaminants such as methylene blue dye from water. This approach offers a sustainable method for managing phytoremediation biomass while simultaneously contributing to water purification.

Keywords: Adsorption, Adsorption isotherms, Biochar, Phytoremediation, Thermodynamic studies

1 Introduction

One of Botswana's largest mining companies, Bamangwato Concessions Limited (BCL), was founded in the late 1950s to exploit the copper-nickel resources in Selebi-Phikwe. Full-scale mining and smelting began in the early 1970s and continued for more than 40 years [1]. Significant environmental pollution was produced by the mine and smelter during its operation, including the release of large amounts of sulphur dioxide (SO_2) into the atmosphere, which caused vegetation damage, acid deposition, and a decline in air quality [1]. Additionally, heavy metals such as Cu, Ni, Fe, Mn, and Zn accumulated in nearby soils during the mine's operation, causing vegetation damage and environmental degradation [2]. Elevated metal concentrations and poor land quality in and around Selebi-Phikwe were caused by wastewater discharges and mine tailings, which also presented threats of water contamination from acid mine drainage [1], [2]. Due to prolonged low global copper and nickel prices, declining ore grades, high operating and

Applied Science and Engineering Progress, Vol. 20, No. 3, 2027, 8259

smelting costs, and sustained financial losses of over $713 million, the BCL mine ceased operations in 2016 and was placed under liquidation in 2017 [1], [2]. However, the company left significant environmental legacies that still require monitoring and remediation.

Phytoremediation plants can remediate acid mine drainage (AMD) and AMD-affected soils due to their strong adaptability to extreme toxic environments [3]. They hyperaccumulate toxins from AMD and AMD soils, thereby reducing environmental contamination [4]. Phytoremediation is an environmentally friendly, green, and cost-efficient technology that employs plant processes and their associated rhizospheric microorganisms to contain, chelate and immobilize contaminants like heavy metals into less toxic metal organic complexes stored in vacuoles [5], [6]. *Cyperus papyrus* (CP) and *Phragmites australis* (PA) are phytoremediation plants growing in the BCL mine tailings.

During and after phytoremediation, toxic substances present in the biomass may enter the food chain via domestic animals if the plants are not properly contained [7]. Furthermore, biomass harvested from phytoremediation sites requires appropriate handling to prevent secondary environmental pollution [4]. Therefore, identifying sustainable strategies for managing phytoremediation waste biomass is essential. This study seeks to explore an environmentally friendly and sustainable application of biomass from phytoremediation plants. Pyrolysis has gained interest in research as a technique commonly employed in the utilization of bio-waste [8]. Feedstock materials are typically carbon-based, including biomass, plastics, coal, and carbon waste [8]. Biochar produced by pyrolysis can be used as an adsorbent to remove toxic contaminants from water, including inorganic compounds and organic dyes such as methylene blue [9].

Although biochar-based adsorption of methylene blue has been widely investigated, few studies have explored the utilization of heavy metal contaminated phytoremediation biomass as precursors for adsorbent production. This study presents a dual benefit approach by addressing the disposal challenges of contaminated biomass harvested from mine tailings while simultaneously producing value added biochar for wastewater remediation. To the best of our knowledge, this is the first comparative investigation of biochar derived from CP and PA from BCL mine tailings for methylene blue adsorption.

The primary objective of this research is to utilize biochar produced from valorized phytoremediation biomass waste collected from BCL mine tailings, acid mine drainage and soils in the vicinity of the mine, for the adsorption of methylene blue from aqueous solutions. The study examines the effects of several operational parameters, including contact time, adsorbent dosage, temperature, and initial methylene blue concentration, on the adsorption performance. Furthermore, the adsorption behavior is assessed through kinetic and thermodynamic analyses.

2 Materials and Methods

2.1 *Chemicals*

Methylene blue, hydrochloric acid (HCl), nitric acid (HNO_3), sodium nitrate ($NaNO_3$), activated charcoal and sodium hydroxide (NaOH) were purchased from Alpha Chemika, India.

2.2 *Sampling*

Phragmites australis and *Cyperus papyrus* species used in this study were harvested in the heavy metal-laden Selibe-Phikwe BCL mine tailings, acid mine drainage, and soils in the vicinity of the mine. The geographical coordinates for collecting *Phragmites australis* were 21.92638° S, 27.86828° E, and for *Cyperus papyrus* were 21.92675° S, 27.86896° E. The plants were randomly sampled around the area and cut at about 15 cm above ground level, using plant shears. Both plants were transported in 50-kilogram woven polypropylene sacks. Before further processing, the biomass was air-dried for 14 days and subsequently oven-dried at 105 °C for 72 hours. The dried material was then reduced in size by cutting into smaller pieces for pyrolysis. Soil samples from the root zones of both plant species were also collected, at 10 cm below ground level and stored in polyethylene sampling bags for further analysis.

2.3 *Biochar production*

The biomass was pyrolysed in an in-house pyrolysis plant at the Botswana International University of Science and Technology, Chemical Engineering Laboratory. The pyrolytic temperature was 550 ℃ in a N_2 atmosphere at a gas flow rate of 8.2 m^3/hr. Pyrolysis was conducted until the reaction went to

Applied Science and Engineering Progress, Vol. 20, No. 3, 2027, 8259

completion after 70 minutes. The biochar was then placed in deionized water and then agitated at 200 rpm in a Stuart Orbital Shaker, China, for 24 hrs to remove impurities. After washing, the biomass was dried at 105 ℃ for 24 hrs in an oven.

The resultant biochar was post-activated by agitation in an orbital shaker at 200 rpm for 24 hrs at a mass-to-volume ratio of 1:20 (g: mL) using 0.1 M KOH, HCl, $MgCl_2$, and H_2O_2 as the activating agents. The samples were then filtered and washed with deionized water to remove the excess activation reagents. The samples were washed again with 500 mL of 0.1 M HCl, for basic reagents, and 0.1 M NaOH for acidic reagents, by agitating for 30 minutes at 200 rpm in an orbital shaker. Thereafter, it was filtered and rinsed with deionized water for another 30 minutes at a mass-to-liquid ratio of 1:20 (g: mL). The samples were then filtered and dried in an oven for 24 hrs at 105 °C, followed by crushing with a mortar and pestle, and then sieved with a 150 µm ASTM E11 ELE International laboratory test sieve (United Kingdom).

2.4 *Physicochemical analysis and characterization*

2.4.1 Heavy metal analysis

To determine the concentrations of heavy metals in the soils, biochar, and plant biomass, the soils, biochar, and biomass were digested using an aqua regia solution prepared at a 3:1 vol/vol HCl: HNO_3 ratio. The samples were digested as follows: 10 mL of aqua regia solution was separately added to 0.1 g of the soils, and 0.5 g of the biomasses and biochars. The mixtures were heated on a hot plate in a fume hood at 95 ℃ for 30 minutes. For the biomass samples, 2 mL of H_2O_2 was added to digest the organic matrix. After all the solids had dissolved, the samples were left to cool before filtration with 0.45 µm syringe filters for heavy metal (HM) analysis. The analysis of heavy metals (Cu, Ni, Mn and Zn) was done using a Thermo Scientific iCAP 7400 Duo Inductively Coupled Plasma - Optical Emission Spectrometer (ICP-OES) from China. A 5-point instrument calibration process was carried out using ICP-OES calibration standard solutions in the range of 0.1-5.0 mg/L. Leaching tests of the HMs from biomass and biochar were done using deionized water at 298.15 K at a solid: liquid ratio of 1:20 (g: mL) by oscillation for 24 hrs in an orbital shaker at a speed of 200 rpm.

2.4.2 pH, electrical conductivity, and total dissolved solids

Water suspensions of the samples were prepared at 298.15 K using a solid: liquid ratio of 1 g: 20 mL. The suspensions were agitated for 2 hrs at 200 rpm in an orbital shaker and thereafter tested for pH, EC, and TDS. The instrument used for analysis of EC and TDS was a SensION+ EC7, Hach Lange S:L:U electric conductor (Germany). The instrument used to measure pH was a Thermo Scientific ORIONSTAR AIII pH meter (USA).

2.4.3 Biochar characterization

The phase composition and crystal structure of the samples were analyzed using a Bruker D8 Advance Cu-Kα X-ray diffractometer (XRD), Germany. The values of 2θ were between 5 and 90 degrees and the step size was 0.02 degrees, with a time of 0.200 sec/step. A Fourier transform infrared (FTIR) spectrometer (Vertex 70v), Germany, was used for functional groups analysis. For the examination of the sample's surface properties and microstructure, a Scanning Electron Microscope (SEM) from ZEISS Sigma, Germany, was used. The magnification used was 10,000X. For the determination of specific surface area and pore size distribution, the BET surface area analyzer (Anton Paar GmbH NOVA 800, Australia) was used.

2.4.4 Surface charge analysis

The point of zero charge (PZC) for the biochar was determined using the salt addition method, with sodium nitrate ($NaNO_3$) serving as the electrolyte [10]. An adsorbent mass of 0.2 g was added to 40 mL of 0.1 M $NaNO_3$ solution, with initial pH (pH_i) values ranging from 1 to 12. The samples were tightly sealed in reagent bottles and agitated at 200 rpm in an orbital shaker for 24 hours at a temperature of 298.15 K, after which the final pH (pH_f) was recorded. The change in pH, ΔpH (pH_f - pH_i), was plotted against the initial pH and the point of zero charge was recorded as the initial pH, where the ΔpH was zero

2.5 Batch adsorption studies

To evaluate the effects of contact time, adsorbent dosage, solution pH, temperature, and initial methylene blue (MB) concentration, adsorption

Applied Science and Engineering Progress, Vol. 20, No. 3, 2027, 8259

studies were conducted in capped glass vials. During each experiment, 25 mg of biochar was mixed with 20 mL of a 50 mg/L MB solution at pH 7, except when the specific parameter under investigation was varied. The suspensions were agitated to reach equilibrium for 7 days. After attainment of equilibrium, the mixtures were centrifuged at 14,000 rpm for 4 minutes. The supernatant was carefully transferred into a quartz cuvette, and the residual MB concentration was determined using a UV–visible spectrophotometer at the maximum MB absorption wavelength (λmax) of 662 nm. Quantification was performed using a five-point calibration curve. Adsorption capacity (mg/g) and adsorption efficiency (%) were calculated using Equations (1 and 2).

$$Adsorption\ capacity\ (q_e) = \frac{(C_o - C_e)V}{W} \quad (1)$$

$$Adsorption\ efficiency\ (\%) = \frac{(C_o - C_e)}{C_o} \times 100\ \% \quad (2)$$

Where C_o represents the initial concentration of methylene blue in mg/L, C_e denotes the equilibrium concentration in mg/L, q_e is the equilibrium adsorption capacity expressed in mg/g, W is the mass of the adsorbent (g), and V is the solution volume (L).

2.5.1 Adsorption isotherm experiments

Methylene blue (MB) solutions of varying concentrations ranging from 20 to 1008 mg/L were used in batch adsorption experiments. A mass of 25 mg of the adsorbent was added to 20 mL of MB solution at pH 7 in glass vials. The mixtures were shaken at 200 rpm in an orbital shaker maintained at 298.15 K for 7 days. Following agitation, the suspensions were centrifuged at 14,000 rpm for 4 minutes, and the supernatant was analyzed using a UV-visible spectrophotometer to determine the residual MB concentration. To evaluate the adsorption characteristics of MB onto the biochar, the equilibrium data were fitted to three widely used isotherm models: Langmuir, Freundlich, and Temkin models. Nonlinear regression analysis was applied to fit the data to the models, and the best fitting model was selected based on the lowest sum of squared residuals (SSR). The mathematical formulae of these models are provided in Table 1. The separation factor was calculated using Equation 3.

Table 1: Adsorption isotherm models applied in this study.

Adsorption isotherms	Non-linear equations
Langmuir	$q_e = \frac{q_m . K_L . C_e}{1 + K_L . C_e}$
Freundlich	$q_e = K_F . C_e^{\ 1/n}$
Temkin	$q_e = \frac{R_T}{b_T} ln\ (K_T . C_e)$

$$Separation\ factor\ (R_L) = \frac{1}{1 + K_L C_O} \quad (3)$$

Where q_e (mg/g) denotes the equilibrium adsorption capacity and C_e (mg/L) represents the solute concentration at equilibrium. The constants K_L, K_F, and K_T correspond to the Langmuir, Freundlich, and Temkin models, respectively, and are associated with adsorption capacity and performance. The Langmuir constant K_L reflects the affinity between the adsorbate and adsorbent, with higher values indicating stronger interactions.

Similarly, a larger K_F value suggests greater adsorption capacity [11]. An increase in the Temkin constant K_T with temperature may imply enhanced adsorption strength at the adsorbent surface [12]. The parameter q_m (mg/g) represents the maximum monolayer adsorption capacity and is an important indicator of adsorbent performance. C_0 is the initial solute concentration (mg/L), while (R_T/b_T) is the Temkin constant that is associated with the heat of adsorption. The term 1/n describes adsorption intensity or surface heterogeneity; values within the range $0.1 < 1/n < 1.0$ indicate favorable adsorption conditions [12].

2.5.2 Kinetic adsorption experiments

MB solutions with initial concentrations of 50 mg/L at pH 7 were contacted with the biochar adsorbents at a mass-to-volume ratio of 1:800 (mg: mL). The systems were evaluated at four temperatures: 298.15, 308.15, 318.15, and 328.15 K, up to the equilibrium time of seven days. Residual MB concentrations at predetermined time intervals were measured using the procedure described in the batch adsorption experiments. To interpret and predict the adsorption behavior, the experimental data were fitted to four kinetic models representing adsorption at active sites as well as external and internal diffusion mechanisms. These models are the pseudo-first-order, pseudo-second-order, intraparticle diffusion, and Elovich models. Their mathematical

expressions are provided in Table 2. Model suitability was evaluated using the sum of squared residuals (SSR).

In these models, q_t (mg/g) represents the amount of MB adsorbed at time t (minutes), and q_e (mg/g) is the adsorption capacity at equilibrium. The constants k_1 and k_2 correspond to the pseudo-first-order and pseudo-second-order rate constants, respectively. For the intraparticle diffusion model, K_{diff} is the intraparticle diffusion rate constant, while C is associated with boundary layer thickness. Within the Elovich model, α represents the initial adsorption rate, and β relates to the extent of surface coverage during chemisorption. The reciprocal term 1/β provides an estimate of the number of available adsorption sites [13]-[15].

Table 2: Adsorption kinetic model equations used.

Adsorption kinetic model	Non-linear equation
PFO	$q_e = q_e(1 - e^{-k_1 t})$
PSO	$q_t = \frac{k_2 q_e^2 t}{1 + k_2 q_e t}$
Elovich	$q_t = \frac{1}{\beta} + ln(\alpha\beta t + 1)$
Intraparticle diffusion	$q_t = K_{diff} \times t^{1/2} + C$

2.5.3 Thermodynamic studies

The thermodynamic parameters (standard Gibbs free energy change, standard entropy change, and standard enthalpy change) were calculated using Equations (4)-(5).

$$\Delta G° = -RTlnK \quad (4)$$

$$lnK = -\frac{\Delta H°}{RT} + \frac{\Delta S°}{R} \quad (5)$$

Where the standard Gibbs free energy change is represented by ΔG°, the absolute temperature is represented by T, while the equilibrium constant is represented by K, and R represents the gas constant. Furthermore, the standard enthalpy change (ΔH°) and standard entropy change (ΔS°) were derived from the slope and intercept of a linear plot of ln K versus 1/T (Equation 5). The equilibrium constant, K, was calculated using Equation 6, after modification of the equation $K=q_e/C_e$ from Ahmed *et al.,* (2025) [16] , which was also derived from the fundamental relationship expressed in Equation 7, into a dimensionless quantity.

$$K = \frac{q_e}{C_e} \times MW\ (MB) \times [adsorbate]^0 \quad (6)$$

$[adsorbate]^0$ = standard concentration of the adsorbate (mol/L)

$$\frac{C_e}{q_e} = \frac{1}{q_m K_L} + \frac{C_e}{q_m} \quad (7)$$

Where K_L is the Langmuir constant (L/mg), q_e is the adsorption capacity at equilibrium (mg/g), C_e is the solute equilibrium concentration (mg/L), q_m is the maximum adsorption capacity (mg/g) and MW is the molecular weight of methylene blue (g/mol).

2.6 *Regeneration*

Spent biochar adsorbents were regenerated by washing with deionized water for 120 minutes in an orbital shaker operating at 200 rpm and 298.15 K, at a weight: volume ratio of 1: 100 (g: mL). The washed materials were separated by gravity filtration and oven-dried at 105 °C for 24 hrs. This regeneration approach was intentionally designed to avoid the use of additional chemical reagents.

2.7 *Statistical analysis of the data*

Analysis of variance (ANOVA) was performed using R software to assess the statistical significance of differences. All experiments were conducted in triplicate, and the reported values represent the mean, with error bars indicating the standard deviation (SD).

3 Results and Discussion

3.1 *Biochar characterization*

Activating agents HCl, $MgCl_2$, H_2O_2, and KOH gave removal efficiencies of 10.1, 6.1, 59.6, and 63.0 %, respectively, for CP biochar and 5.5, 28.9, 46.1, and 29.1%, respectively, for PA biochar. Thus, KOH was adopted as the activation agent for CP biochar, and H_2O_2 was adopted for PA biochar. The activated biochars are referred to herein as CP-KOH and PA- H_2O_2. KOH is considered a good activation agent because it increases micro/mesopores, enlarging the pore network on the adsorbent, thereby increasing the surface area. This has been attributed to the release of CO_2 and CO during the reaction of KOH and biochar carbon surface, even though it has etching behaviour that can destroy

structures of weak adsorbents like PA plants [17], [18]. Xie *et al.,* (2022) observed a high density of micropores in KOH-activated biochar [19]. On the other hand, hydrogen peroxide (H_2O_2) oxidizes the carbon surface, generating hydroxyl, carbonyl, and carboxyl groups. It increases the surface polarity and enhances electrostatic attraction and hydrogen bonding [20], [21].

Figure 1 (a-b) shows the XRD patterns of CP-KOH and PA- H_2O_2 biochars, with broad diffraction peaks centered at $2\theta \approx 21.9$ ° and 23.4 °, respectively. These values fall within the typical 20-26° range for the (002) carbon plane, which reflects graphitic structures and the random stacking of coherent aromatic graphene layers [22], [23]. Another broad hump at $2\theta \approx 43$ ° corresponds to the (100) plane, reflecting the in-plane sp^2-carbon hexagonal network. These two broad peaks indicate an absence of a highly ordered, long-range crystalline structure in both activated biochars [24]. Weak peaks at 28.4° and 40.5° observed for CP-KOH biochar (Figure 1 (a)) may be attributed to inorganic phases such as quartz (SiO_2) or potassium-containing compounds from incomplete removal of activating agents [23], [25], [26].

Figure 2 shows the FTIR spectra of CP-KOH and PA-H_2O_2 biochars before and after methylene blue adsorption. Broad peaks observed at 3442 cm^{-1} for CP-KOH and 3432 cm^{-1} for PA-H_2O_2 correspond to O-H stretching vibrations, with changes in intensity after adsorption indicating the involvement of hydroxyl groups in hydrogen bonding with MB [27]. Weak bands at 2973 and 2943 cm^{-1} were assigned to aliphatic C-H, -CH_2, and CH_3 stretching bands, with reduced intensity after adsorption, suggesting electron transfer or π-π interactions with the biochar surface [28]. Both CP-KOH and PA-H_2O_2 showed an inverted peak at 2354 and 2345 cm^{-1}, respectively, which could have been due to background subtraction error. These bands were attributed to asymmetric C=O stretching modes of CO_2 [18]. The peaks at 1605 cm^{-1} (CP-KOH) and 1603 cm^{-1} (PA-H_2O_2), assigned to aromatic C=C and carbonyl (C=O) stretching modes, shifted to higher wavenumbers after adsorption, indicating π-π interactions between methylene blue aromatic rings and the biochar surface. Similarly, reduced peak intensities at 1386 and 1383 cm^{-1}, associated with C-O stretching modes, confirm their participation in electrostatic interactions during adsorption [12], [13].

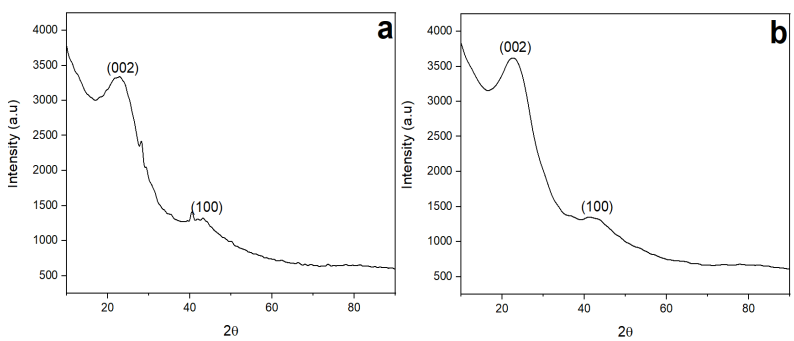

Figure 1: XRD spectra for CP-KOH biochar (a) and PA-H_2O_2 biochar (b).

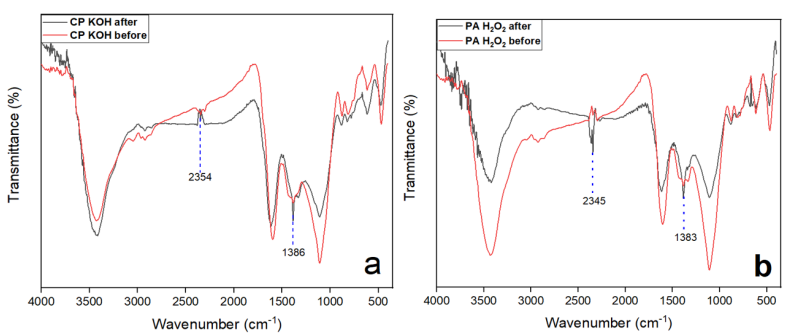

Figure 2: FTIR spectra of CP-KOH (a) and PA- H_2O_2 (b) activated biochar before and after adsorption of MB.

The SEM images of the biochars in Figure 3 show well-defined pores with interconnected voids and channels, normally seen in biochar produced from the pyrolysis of biomass, where the cell walls and vascular structures collapse, leaving interconnected openings [14], [15].The images depict three-dimensional heterogeneous micro-macro pores at a magnification of 10000X and aperture size of 30.00 µm. Channels and voids could be created when the remaining carbonaceous matrix shrinks and cracks as compounds like CH_4, CO_2, and $H_2O(g)$ escape during thermal decomposition of biomass [29]. As this happens, meso, micro and macro pores are produced [29]. Biochar SEM images usually show cylindrical and polygonal pores, interspersed with several large pores. These same structures are seen in Figure 3.

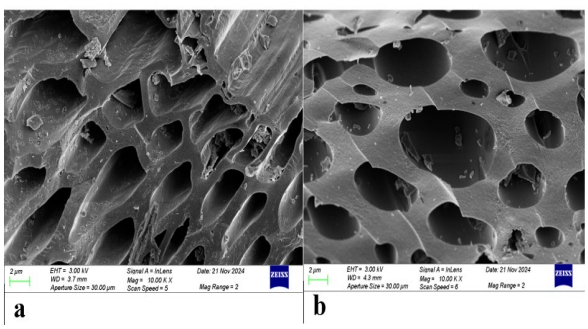

Figure 3: SEM micrographs of (a) CP-KOH biochar and (b) PA-H_2O_2 activated biochar, both at 10,000X magnification.

The Brunauer-Emmett-Teller (BET) analysis was also applied for the determination of porosity as well as to evaluate the specific surface area of the materials, as indicated in Table 3. CP-KOH had a pore diameter of 3.22 nm, while PA-H_2O_2 had a pore diameter of 3.23 nm. On the other hand, the surface area of CP-KOH biochar was 6.19 m^2/g, higher than that of PA-H_2O_2 biochar at 2.95 m^2/g. The pore types in BET are classified based on the IUPAC classification as: pore sizes <2 nm are micropores, those between 2-50 nm are mesopores, while macropores are >50 nm [30]. The pores of both CP-KOH and PA- H_2O_2 adsorbents used in this study were identified as mesopores [31].

3.2 *Chemical characteristics of phytoremediation biomass and biochar*

3.2.1 pH, EC, and TDS for acid mine drainage soil where the plant samples were obtained.

The AMD soils in which the biomass was growing are herein referred to as AMD-CP for the soil in which CP was collected and AMD-PA for the soil in which PA was collected. The pH of AMD-CP was 5.27 and 4.83 for AMD-PA, indicating very acidic conditions (Table 4). The acidity may be due to the oxidation/hydrolysis of heavy metals leached from the mine processes and acidic rains caused by the reaction of rainwater with metal particulate matter [32]. These results align well with results in a study by Manyiwa *et al.,* (2022), [7]. However, phytoremediation plants are able to survive in such highly acidic soils due to their plant processes, including hyperaccumulation, phytostabilization, phytodegradation, and rhizofiltration [3], [33].

The electrical conductivity of AMD-CP was 4713 ± 12 mS/cm and for AMD-PA was 4853 ± 5 mS/cm, whereas the total dissolved solids for AMD-CP and AMD-PA were 2343 ± 6 and 2420 ± 10 mg/kg, respectively. The high EC and TDS could have been influenced by the vast amounts of heavy metal ions from mining processes on top of sulphur-containing minerals, which influence the formation of acid mine drainage [34]. High concentrations of these ions increase the ability of water to conduct electricity [35].

Table 3: Physicochemical properties of CP-KOH and PA- H_2O_2, obtained from BET surface area analysis.

Physiochemical index	CP-KOH	PA-H_2O_2
BET Surface Area (m^2/g)	6.19	2.59
Pore volume (cm^3/g)	0.00202	0.00816
Pore diameter (nm)	3.22	3.23

Table 4: Chemical characteristics of the acid mine drainage.

AMD samples	for	pH	EC (mS/cm)	TDS (mg/kg)
AMD-CP		5.27 ± 0.06	4713 ± 12	2343 ± 6
AMD-PA		4.83 ± 0.06	4853 ± 5	2420 ± 10
p-values				
Replicates		0.999_{ns}	0.997_{ns}	0.975_{ns}
Biomass	×	0.999_{ns}	0.998_{ns}	0.987_{ns}
Biomass				

H_0 = There is no significant difference in mean pH, EC, and TDS between the replicates and biomasses. *p*-value < 0.05 = highly significant, reject H_0, *p*-value > 0.05 = not significant (ns), fail to reject H_0.

Applied Science and Engineering Progress, Vol. 20, No. 3, 2027, 8259

3.2.2 pH of the phytoremediation biomasses and biochar

The results in Table 5 show an increase in the pH after the biomass was pyrolyzed to biochar. The pH for the plant samples was in the same range as the acid mine drainage soils in which they grew. The pH was 5.37 ± 0.06 for CP biomass and 5.2 ± 0.2 for PA biomass, as shown in Table 5.

Table 5: pH of the phytoremediation biomasses and biochar.

Samples	pH
CP biomass	5.37 ± 0.06
PA biomass	5.2 ± 0.2
CP biochar inactivated (CPB)	7.7 ± 0.1
PA biochar inactivated (PAB)	7.6 ± 0.2
Non-phytoremediation CP	8.47 ± 0.04
Non-phytoremediation PA	7.98 ± 0.08
p-values	
Replicates	0.999_{ns}
Biomass × Biomass	0.934_{ns}
Biochar × Biochar	0.912_{ns}

H_0 = There is no significant difference in mean pH between the replicates, biochars and biomasses. *p*-value < 0.05 = highly significant, reject H0, *p*-value > 0.05 = not significant (ns), fail to reject H_0.

The stored heavy metals accumulated during the phytoremediation process could have been leached into water and their subsequent hydrolysis, resulting in the acidic pH obtained [3]. This explains the need for proper handling of the waste biomass. After pyrolysis, the biochar suspensions gave a pH of 7.7 ± 0.1 for CP-inactivated and 7.6 ± 0.1 for PA-inactivated. The increase in pH after pyrolysis could have been a result of a decrease in organic functional groups such as -COOH and -OH at high pyrolytic temperatures [36]. In biochar produced at higher pyrolysis temperatures, the degradation of acidic functional groups, including phenolic and carboxylic moieties, significantly contributes to the observed increase in pH [36]. As a result, the biochar will not reduce the pH of the water during adsorption.

3.2.3 Heavy metal analysis

The results in Table 6 show that Cu and Ni were present in high concentrations in all samples, compared to Zn and Mn. The high concentration of Cu and Ni in the soils was because the Selibe Phikwe BCL mine mined Cu and Ni, resulting in the deposition of mine tailings with high concentrations of Cu and Ni over the years of its operation [37]. The results show that the concentrations of HM bioaccumulated by the phytoremediation *Cyperus papyrus* biomass (PCPB) and *Phragmites australis* biomass (PPAB) were independent of the HM concentrations in the soils. This was due to the hyperaccumulation tendencies of the plant species, which were investigated in a study by Ishmael *et al.,* (2024), [38]. Nevertheless, PPAB had concentrations lower than those in the soil for Cu, Mn, and Ni, except for Zn, where it had a higher concentration of 12.000 ± 0.005 mg/kg compared to 1.240 ± 0.002 mg/kg in the soil. This means the hyperaccumulation abilities

Table 6: Concentration of metals in the AMD soils, phytoremediation biomass and biochar.

Sample	Cu (mg/kg)	Mn (mg/kg)	Ni (mg/kg)	Zn (mg/kg)
CP soil	27 ± 3	7.7 ± 0.5	10.7 ± 0.1	8.1 ± 0.3
PA soil	1350 ± 50	53 ± 2	205 ± 5	31 ± 1
PCPB	6.9 ± 0.5	2.8 ± 0.2	3.01 ± 0.09	3.27 ± 0.07
PPAB	4.2 ± 0.2	2.67 ± 0.07	1.50 ± 0.06	12.0 ± 0.5
CPB	3.09 ± 0.09	0.4 ± 0.2	0.61 ± 0.04	2.56 ± 0.05
PAB	3.4 ± 0.1	1.61 ± 0.03	0.16 ± 0.01	5.3 ± 0.1
p-values				
Replicates	0.999_{ns}	0.999_{ns}	0.999_{ns}	0.993_{ns}
Biomass × Biomass	<0.0001***	0.475_{ns}	<0.0001***	<0.0001***
Soil × Soil	<0.0001***	<0.0001***	<0.0001***	<0.0001***
Biochar × Biochar	0.135ns	<0.0001***	<0.0001***	<0.0001***
Biochar × Biomass	<0.0001***	<0.0001***	<0.0001***	<0.0001***

CPB: phytoremediation Cyperus papyrus biomass. PPAB: phytoremediation Phragmites australis biomass. CPB: Cyperus papyrus biochar. PAB: Phragmites australis biochar. H_0 = There is no significant difference in mean metal concentration between the replicates and biomass. *p*-value < 0.05 = highly significant, reject H0, *p*-value > 0.05 = not significant (ns), fail to reject H_0

of PPAB were less than those of PCPB for most metals investigated in this study [39], [40].

The biochar for both plant species had concentrations less than those of both the phytoremediation biomasses and the AMD soils. This is because during high pyrolytic temperatures, the heavy metals get transformed into stable oxides or sulfides [41], which are not readily dissociated in the aqua regia media, hence making them less bioavailable, reducing mobility and leaching [29], [42]. With that, biochar was safe for use in the adsorption of organic pollutants with minimal risk of leaching HM in water, supported by results from the leaching test [3]. The leached concentrations of Cu, Ni, Zn and Mn for CP-KOH were 0.00065, 0.0051, 0.0014, and 0.0002 mg/kg, respectively, while the concentrations of leached HM for PA-H_2O_2 biochar in the same order were 0.00052, 0.0030, 0.0014 and 0.0001 mg/kg. A study by Ippolito *et al.,* (2024), [43], also suggests that pyrolysis reduces the mobility of HM as HM-contaminated feedstock is converted into biochar [44].

3.3 *Effects of reaction parameters on methylene blue adsorption*

3.3.1 Effect of time

Figure 4(a) shows the adsorption efficiency of MB onto CP-KOH and PA- H_2O_2 as a function of time under fixed conditions (25 mg adsorbent dosage, pH 7, and 50 mg/L initial MB concentration). Both biochars exhibited rapid initial adsorption within the first 5 min, with removal efficiencies of 50.7 ± 0.3 % for CP-KOH and 40 ± 2 % for PA- H_2O_2, followed by a slower uptake phase until equilibrium was reached after approximately 7 days. At equilibrium, CP-KOH achieved a higher removal efficiency of 87 ± 2 % than PA-H_2O_2 at 80 ± 3 %, reflecting its superior adsorption performance.

The prolonged equilibrium time is considerably longer than the several minutes to hours commonly reported for activated biochars in methylene blue adsorption studies [45], [46]. A recent study by Vasiljevi´c *et al.,* [47] on the adsorption of methylene blue by commercial activated carbon indicates that equilibrium was reached in the first 20 minutes with 25 mg of the adsorbent in 25 mg/L MB. Other studies also found equilibrium time of less than 90 minutes with the same adsorbate: adsorbent ratio used in this study [48], [49]. This corresponds to the results obtained for the same adsorption of methylene blue by commercial activated carbon, as reported in Figure 4(b). Even so, some studies have reported a long equilibrium time for the adsorption of MB on activated biochar [46], [50]. The Weber-Morris intraparticle diffusion model plots have been used to explain the potential diffusion and boundary layer limitations (see section 3.3.6), leading to longer equilibrium times [50].

3.3.2 Effect of the dosage of biochar

Figure 4(c) illustrates the influence of CP-KOH and PA-H_2O_2 biochar dosage on MB removal within a range of 10-40 mg. For both adsorbents, adsorption efficiency increased with increasing dosage. In the case of PA-H_2O_2 biochar, only a slight increase in efficiency was observed between 25 mg and 30 mg, followed by a more noticeable rise to 40 mg. The marginal improvement may be attributed to underutilization of adsorption sites, possibly resulting from particle agglomeration. Such aggregation can reduce effective surface area, block pore structures, and ultimately decrease adsorption capacity [51],

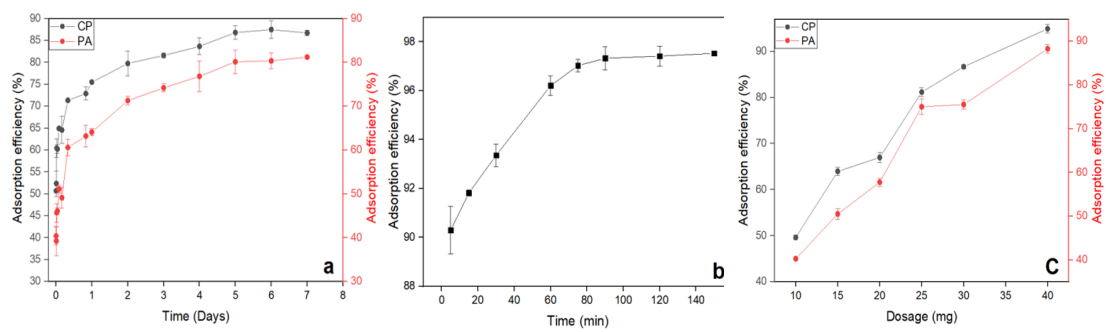

Figure 4: Effect of time (a) on the adsorption efficiency of CP-KOH and PA- H_2O_2 biochar and (b) on commercial activated carbon at a concentration of 50 mg/L and pH 7; (c) is the effect of dosage on the adsorption efficiency of CP-KOH and PA- H_2O_2 biochar.

[52], [53]. A similar trend was observed for CP-KOH biochar within the 25-40 mg range. Despite these observations, both biochars demonstrated an overall increase in adsorption efficiency with higher dosage. This enhancement can be attributed to the greater availability of active adsorption sites, which promotes increased removal of MB from solution [50].

3.3.3 Effect of solution pH on the adsorption of MB on biochar

Figure 5 shows the effects of solution pH, in the pH range of 2 to 12, on methylene blue adsorption onto CP-KOH and PA-H_2O_2 biochars. Adsorption efficiency generally increased with increasing pH for both adsorbents, while the slight variation observed between pH 2 and 3 was not statistically significant (p-value > 0.05). At low pH, adsorption efficiency is low because highly acidic conditions may be attributed to the elevated positive charge density on the adsorbent surface, which can cause electrostatic repulsion of cationic MB molecules [46], [47], [54]. This trend is consistent with the PZC values of 7.9 for CP-KOH and 5.95 for PA-H_2O_2 (Figure 6), which indicate that at pH values below these thresholds, the biochar surfaces are positively charged and electrostatically repel cationic methylene blue molecules, resulting in lower adsorption efficiency [46], [55].

At neutral pH (pH 7), both biochars achieved adsorption efficiencies above 70%, demonstrating effective dye removal under near-neutral conditions. The improved adsorption at higher pH is attributed to surface deprotonation, which enhances electrostatic attraction between negatively charged functional groups and methylene blue molecules [46]. Similar pH-dependent adsorption behavior has been widely reported for methylene blue adsorption onto biochars [47], [54]. Based on these results, pH 7 was selected for subsequent experiments as it provided high adsorption performance without requiring additional pH adjustment for practical application.

Figure 7 illustrates the effects of initial methylene blue concentration from 20-1008 mg/L on the adsorption performance of CP-KOH and PA-H_2O_2 biochars. For both adsorbents, removal efficiency decreased with increasing initial dye concentration, while adsorption capacity increased, consistent with trends widely reported for adsorption studies [54], [56]. For PA-H_2O_2 biochar, removal efficiency declined from 90 ± 2 % at 20 mg/L to 14.8 ± 0.5% at

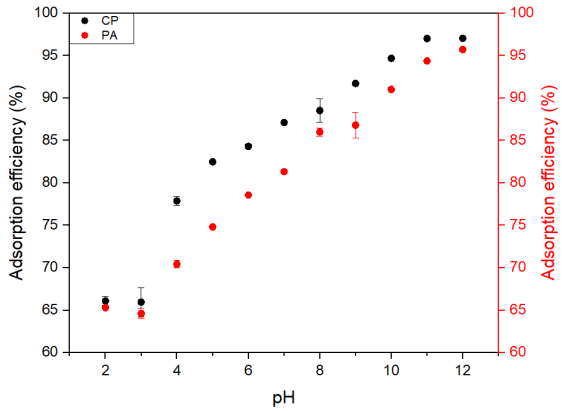

Figure 5: The effects of solution pH on the adsorption of MB on CP-KOH and PA-H_2O_2 biochar at 7 days, 25 mg and 25 °C

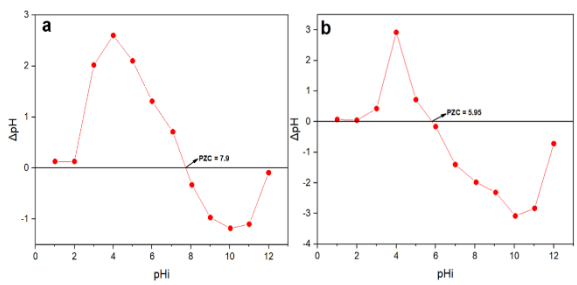

Figure 6: Point of zero charge (PZC) graphs for biochar CP-KOH (a) and PA-H_2O_2 (b)

1008 mg/L, whereas CP-KOH showed a decrease from 97.5 ± 0.8% to 9.1 ± 0.8% over the same concentration range. Despite the reduction in percentage removal, CP-KOH consistently exhibited higher adsorption capacity than PA-H_2O_2, reflecting its superior adsorption affinity.

3.3.4 Effect of initial concentration on CP and PA biochar

The decline in removal efficiency at higher concentrations is attributed to progressive saturation of available adsorption sites, while the increase in adsorption capacity results from the greater mass transfer driving force, provided by elevated methylene blue concentrations [57]. This behavior indicates that although both biochars become less effective in percentage removal at high dye concentrations, their adsorption capacities increase until surface saturation is approached [58].

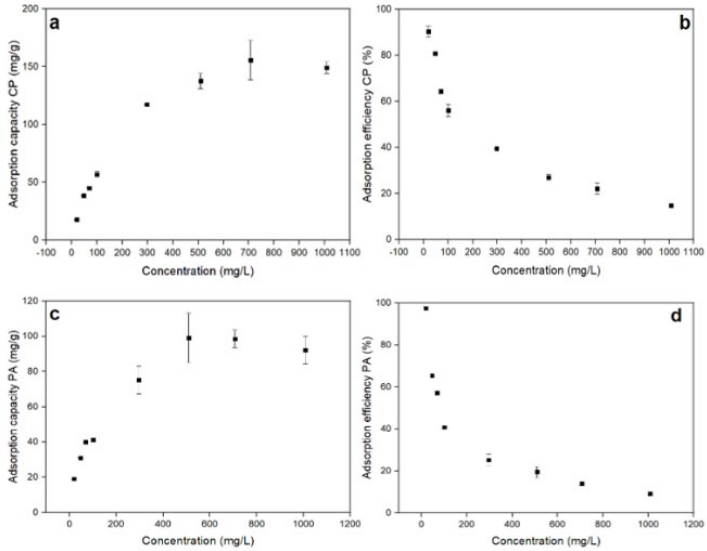

Figure 7: The effect of initial MB concentration on adsorption capacity (a, c) and adsorption efficiency (b, d) for both CP-KOH and PA-H_2O_2 biochar.

3.3.5 Adsorption isotherm studies

The results of nonlinear adsorption isotherm fittings are shown in Table 7. Based on the SSR values in Table 7, the Langmuir model provided the best fit to the experimental data and was selected as the model that describes the adsorption of MB onto both CP-KOH and PA-H_2O_2 biochar adsorbents. CP-KOH biochar had an SSR value of 572 for Langmuir, compared to 750 for the Freundlich and 796 for the Temkin model. On the other hand, PA-H_2O_2 biochar had an SSR value of 297 compared to 3704 for the Freundlich model and 5883 for the Temkin model. Thus, the adsorption process follows the Langmuir model that assumes monolayer adsorption on homogeneous surfaces, as also seen in Figure 8 [59]. The obtained maximum adsorption capacities (q_{max}) for CP-KOH and PA-H_2O_2 biochars were 128.21 and 79.37 mg/g, respectively. The separation factors for biochars were calculated using Equation (3) and values ranged from 0.059 to 0.76 for CP-KOH biochar and from 0.037 to 0.66 for PA-H_2O_2 biochar, indicating favorable and effective adsorption for both biochars [11].

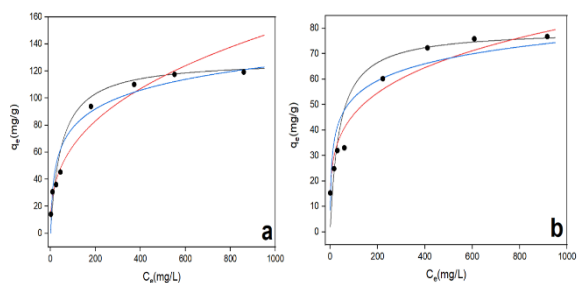

Figure 8: Nonlinear fitting to adsorption isotherm models for CP-KOH (a) and PA-H_2O_2 (b), where the black line represents the Langmuir model, red represents the Freundlich model, blue represents the Temkin model, and black circles represent the experimental data.

Table 7: Isotherm fittings results for the adsorption of MB onto CP-KOH and PA-H_2O_2 adsorbents.

Model	SSR	$K_{(L,F,T)}$	q_{max} (mg/g)	R_L (mg/L)	n	B_T
CP						
Langmuir	572	0.0206	128.21	0.059-0.76	-	-
Freundlich	750	12.1	-	-	0.364	-
Temkin	796	0.512	-	-	-	19.9
PA						
Langmuir	297	0.0259	79.37	0.037-0.66	-	-
Freundlich	3704	15.2	-	-	0.241	-
Temkin	5883	2.45	-	-	-	9.59

3.3.6 *Adsorption kinetic studies*

Figures 9 and 10 represent the results of the nonlinear fitting of experimental kinetic data to the four models evaluated in this study. Kinetic experiments were performed at 298.15, 308.15, 318.15, and 328.15 K. According to Tables 8 and 9, the Elovich model provided the best fit across all temperatures, as evidenced by the lowest SSR values compared to the other kinetic models. For CP-KOH biochar, the SSR values obtained using the Elovich model were 10.04, 23.80, 18.12, and 16.99 at 298.15, 308.15, 318.15, and 328.15 K, respectively. For PA-H_2O_2 biochar, the corresponding SSR values were 49.76, 42.50, 63.71, and 60.39. The Elovich model applies to heterogeneous surfaces and primarily explains chemisorption, with the adsorption rate decreasing exponentially with increasing surface coverage [46], [50]. This means that adsorption can be fast at the beginning, when there are more vacant, high-energy active sites, and as more active sites become occupied, the process shifts to lower-energy sites, and the adsorption rate becomes relatively slow over time [60]. This potentially explains the high equilibrium time of 7 days, suggesting that the rate-limiting step is not a simple diffusion but slow surface reactions and progressive site energy changes [61]. Similar results were obtained by [46], [50], [59]. Given that the adopted adsorption isotherm models suggest monolayer coverage, this suggests that the system was not perfectly homogeneous, yet still reached a monolayer, or near-monolayer, saturation capacity.

Relatively long equilibrium times are routinely explained by fitting the experimental data to the Weber-Morris model to eliminate potential mass transfer or initial diffusion limitations. Figure 11 shows the fit of experimental data to the Weber-Morris model [50].

The initial steep region corresponds to rapid external mass transfer (film diffusion), while the following gradual linear region (middle segment) indicates that intraparticle diffusion became the rate-limiting step [46], representing the gradual migration of the adsorbate into the internal pores of the material, and the final step indicates reduced adsorption rates as the active sites become saturated and equilibrium is approached [59].

The plots were non-linear and did not pass through the origin, indicating that mechanisms other than intraparticle diffusion were involved, and the large values of the intercepts suggest significant boundary-layer resistance during the early stage of

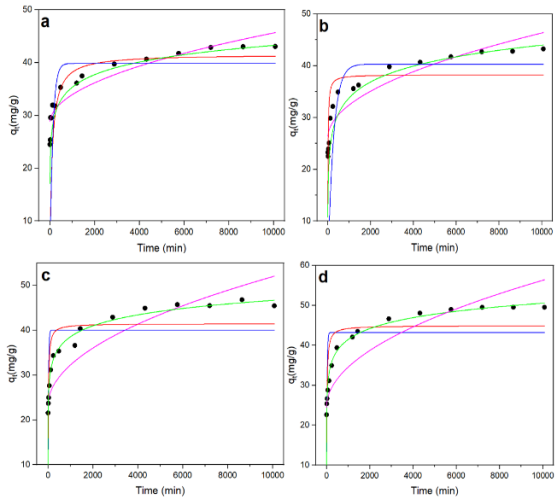

Figure 9: Nonlinear model fitting of various kinetic models for CP-KOH at 298.15 (a), 308.15 (b), 318.15 (c), and 328.15 K (d), where the blue line represents the PFO model, the red line represents the PSO model, the green line represents the Elovich model, the purple line represents the Intraparticle diffusion model, and the black circles represent the experimental data.

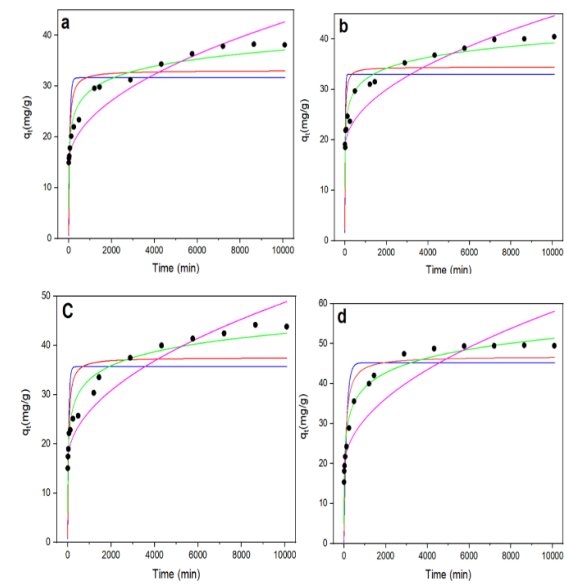

Figure 10: Nonlinear model fitting of various kinetic models for PA-H_2O_2 at 298.15 (a), 308.15 (b), 318.15 (c), and 328.15 K (d), where the blue line represents the PFO model, the red line represents the PSO model, the green line represents the Elovich model, the purple line represents the Intraparticle diffusion model, and the black circles represent the experimental data.

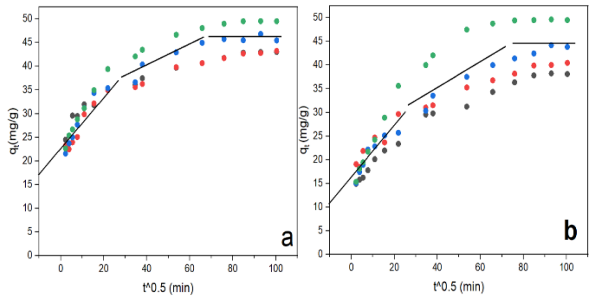

Figure 11: Fitting plots of the intraparticle diffusion model for CP-KOH (a) and PA-H_2O_2 (b), where the black circles represent 298.15 K, red circles represent 308.15 K, blue circles represent 318.15 K, and green circles represent 328.15 K, and the continuous lines represent the Weber-Morries model for reference temp 318.15 K.

adsorption [59]. However, the initial adsorption factor (R_i) was calculated, and for both biochars, R_i was $0.9< R_i >0.5$, indicating that boundary layer diffusion was not the major limiting step [50].

This suggests that as adsorption progresses, the rate decreases due to diffusion resistance within the internal pore structure (intraparticle diffusion limitations), indicating that adsorbate molecules require more time to access deeper active sites [46]. The Elovich model's good fit further supports this. In this system, easily accessible sites were occupied first, followed by slower adsorption onto less accessible, high-energy sites, thereby extending the time required to reach equilibrium.

3.4 *Thermodynamic studies (biochar)*

Thermodynamic parameters for the adsorption process are shown in Table 10. The standard Gibbs free energy change values obtained were -18.84, -19.56, -21.39, and -28.76 kJ/mol for CP-KOH biochar and -17.20, -18.50, -20.47, and -28.65 kJ/mol for PA-H_2O_2 biochar at temperatures 298.15, 308.15, 318.15, and 328.15 K (Table 10). These results indicate that the adsorption of MB on both CP-KOH and PA-H_2O_2 was a spontaneous and feasible process. It has been noted that the adsorption of MB on biochar usually gives $\Delta G°$ values between -20 and 0 kJ/mol, indicating physisorption [62]. However, an analysis of both the adsorption isotherm study and the kinetic study indicates that the process was a complex process with some degree of physisorption and chemisorption. This could suggest a complex mechanism, like ion exchange or surface complexation [63].

In addition, CP-KOH biochar yielded values of +74.17 kJ.mol^{-1} and +307.55 J.mol^{-1}K^{-1} for $\Delta H°$ and $\Delta S°$, respectively. PA-H_2O_2 biochar had +89.85 kJ.mol^{-1} and +354.65 J.mol^{-1}K^{-1} for $\Delta H°$ and $\Delta S°$, respectively. This indicates that the adsorption process of methylene blue onto both CP-KOH and PA-H_2O_2 biochar was endothermic and resulted in a more disordered system. Additionally, following the largely positive values of $\Delta H° > +40$ kJ/mol, the adsorption process was suggested to be chemisorption [64].

Table 8: Results for nonlinear fitting of kinetic models at different temperatures for CP-KOH biochar.

Temperature (K)/ Parameters	PFO	PSO	Elovich	Intraparticle Diffusion
298.15				
$q_{e\,(exp)}$ (mg/g)	43.39			
k_1/k_2	0.129	0.000289		
$q_{e\,(cal)}$ (mg/g)	37.03	38.32		
SSR	394.08	236.20	10.04	767.29
308.15				
$q_{e\,(exp)}$ (mg/g)	43.58			
k_1/k_2	0.0613	0.000260		
$q_{e\,(cal)}$ (mg/g)	36.98	38.27		
SSR	583.87	345.93	23.80	694.40
318.15				
$q_{e\,(exp)}$ (mg/g)	47.80			
k_1/k_2	0.0468	0.000258		
$q_{e\,(cal)}$ (mg/g)	40.05	41.46		
SSR	624.83	364.81	18.12	18.12
328.15				
$q_{e\,(exp)}$ (mg/g)	49.62			
k_1/k_2	0.0425	0.000251		
$q_{e\,(cal)}$ (mg/g)	43.20	44.90		
SSR	784.43	451.21	16.99	909.57

Applied Science and Engineering Progress, Vol. 20, No. 3, 2027, 8259

Table 9: Fitting results of kinetic models at different temperatures for PA-H_2O_2 biochar

Temperature (K)/ Parameters	PFO	PSO	Elovich	Intraparticle Diffusion
298.15				
$q_{e\,(exp)}$ (mg/g)	38.58			
k_1/k_2	0.0182	0.000193		
$q_{e\,(cal)}$ (mg/g)	31.64	33.08		
SSR	613.55	401.99	49.76	317.03
308.15				
$q_{e\,(exp)}$ (mg/g)	40.94			
k_1/k_2	0.0488	0.000171		
$q_{e\,(cal)}$ (mg/g)	33.01	34.45		
SSR	610.80	404.41	42.50	447.49
318.15				
$q_{e\,(exp)}$ (mg/g)	44.81			
k_1/k_2	0.0213	0.000162		
$q_{e\,(cal)}$ (mg/g)	35.67	37.56		
SSR	785.98	517.46	63.71	395.15
328.15				
$q_{e\,(exp)}$ (mg/g)	49.64			
k_1/k_2	0.00831	0.000136		
$q_{e\,(cal)}$ (mg/g)	45.23	46.86		
SSR	779.93	459.88	60.39	781.78

Table 10: Thermodynamic parameters for the adsorption of methylene blue onto CP-KOH and PA-H_2O_2 biochar adsorbents.

Sample/ Temp (K)	ΔG° (kJ.mol^{-1})	ΔH° (kJ.mol^{-1})	ΔS° (J.mol^{-1}.K^{-1})
CP-KOH			
298.15	-18.84	+74.17	+307.55
308.15	-19.56		
318.15	-21.39		
328.15	-28.76		
PA-H_2O_2			
298.15	-17.20	+89.85	+354.65
308.15	-18.50		
318.15	-20.47		
328.15	-28.65		

3.5 *Regeneration*

To assess the practical applicability and overall efficiency of the adsorbents for methylene blue removal, regeneration studies were conducted over five successive cycles using deionized water as the washing agent. As illustrated in Figure 12, the adsorption efficiency of both CP-KOH and PA-H_2O_2 biochars progressively decreased over the five regeneration cycles. For CP-KOH biochar, the removal efficiency declined from 87.0 ± 0.6% in the first cycle to 58 ± 2% after the fifth cycle. Likewise, PA-H_2O_2 biochar exhibited a decrease from 81.6 ± 0.6% to 56.9 ± 0.6% across the same number of cycles. This reduction in performance may be attributed to the gradual loss or blockage of active adsorption sites, as some MB molecules could have remained trapped within the pore structure, making complete desorption difficult [65]. Overall, despite the observed decline, both adsorbents maintained reasonably good regeneration performance throughout the five cycles. It has been reported, however, that mild chemical regeneration, such as a low concentration of NaOH, produces better regeneration performance [59].

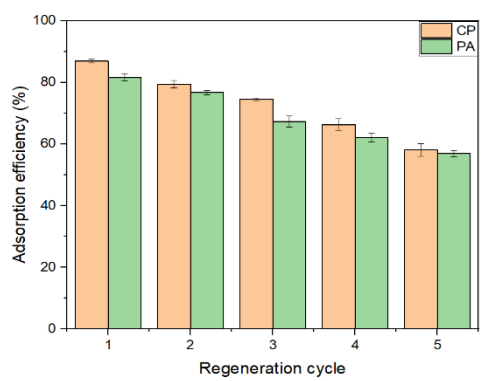

Figure 12: Regeneration cycle of biochar adsorbents.

3.6 *Comparison with other biochar adsorbents*

The adsorption capacities of both biochar materials investigated in this study were evaluated against some adsorbents reported in recent literature (Table 11). While certain adsorbents documented in the literature exhibit higher adsorption capacities, the biochars derived from phytoremediation of CP and PA collected from BCL mine tailings demonstrate considerable potential for methylene blue removal from dye-contaminated wastewater. This is despite the limitation associated with their relatively long equilibrium times. Overall, the findings suggest that biochar produced from phytoremediation biomass sourced from BCL mine tailings is a promising and viable adsorbent for the removal of organic pollutants such as MB from wastewater systems. The high adsorption capacity despite the low BET surface area (Table 3) could be due to the high density of surface functional groups, which in chemisorption may increase the adsorption capacity regardless of the surface area and pore volume [66].

Table 11: Comparing the adsorption capacity of other adsorbents in the adsorption of MB.

Adsorbent	Adsorption capacity (mg/g)	Reference
Rice Straw Biochar	50.27	[67]
Lychee Seed Biochar	124.5	[68]
Biochar from *Phragmites karka*	438.2	[69]
CP-KOH biochar	128.21	This study
PA-H_2O_2 biochar	79.35	This study

4 Conclusions

Biochar derived from phytoremediation waste biomass demonstrated potential for methylene blue adsorption, with CP-KOH showing superior performance to PA-H_2O_2. CP-KOH exhibited a higher adsorption capacity of 128.21 mg/g compared to 79.35 mg/g for PA-H_2O_2, which was attributed to its relatively higher surface area (6.19 m^2/g) compared to PA-H_2O_2 (2.95 m^2/g), as well as its well-developed porous structure. The adsorption data for both biochars were best described by the Langmuir isotherm and Elovich kinetic models, indicating monolayer adsorption on heterogeneous surfaces. FTIR analysis confirmed interactions between methylene blue molecules and surface functional groups. Regeneration studies further demonstrated that both biochars retained adsorption performance over five cycles. The leaching test showed that a very low level of HM metals leached from the biochar, indicating that the thermochemical process of pyrolysis has potential as an alternative sustainable method of handling phytoremediation biomass.

However, the relatively long equilibrium time and low surface area compared to commercial activated carbons suggest limitations for large-scale practical application. Future studies should focus on improving adsorption efficiency through surface modification or activation strategies, optimizing regeneration using mild chemical regenerants, and reducing equilibrium time to enhance process feasibility for wastewater treatment applications. Reduction of equilibration time is key in the alternative utilization of obtained biochar from pyrolysis. Additional processes, such as ball milling to further reduce particle sizes, may be explored in the future. Overall, the findings demonstrate that phytoremediation-derived biochar offers a promising, environmentally sustainable route for waste biomass valorization and dye removal from aqueous systems.

Acknowledgments

Gratitude is sent to the Botswana International University of Science and Technology and the Department of Chemical and Forensic Sciences, for providing facilities and materials to carry out this study. Appreciation also goes to Bamangwato Concessions Limited (BCL) for providing access to the mine tailings for sampling of the biomass adsorbents used in this study. Special thanks to Katlarelo Lenny Sefatlhi for helping with sampling and Michael Olowatosin Bodunrin for assistance in the BET and SEM analysis.

Funding

This research was funded by the [Africa-Japan Collaborative Research SusMine project/ Department of Research, Science, and Technology], grant number [P0081].

Author Contributions

K.M: Methodology, software, formal analysis, and Investigation. S.M: Conceptualization, review, supervision, funding acquisition. P.O: review and editing. V.U: Conceptualization, Supervision, review,

editing, and funding acquisition. All authors have read and agreed to the published version of the manuscript.

Conflicts of Interest

The authors declare no conflict of interest.

Declaration of generative AI and AI-assisted technologies in the writing process

The authors utilized AI tools to enhance the language and readability of the manuscript.

References

[1] B. K. Asare and M. B. K. Darkoh, "Socio-economic and environmental impacts of mining in Botswana: A case study of the Selebi-Phikwe copper-nickel mine," *Eastern Africa Social Science Research Review*, vol. 17, no. 2, pp. 1–41, Jun. 2001.

[2] M. Letshwenyo, "Sulphur and heavy metals contents in soils and *Grewia bicolor* leaves around the Selibe Pikwe Cu-Ni mine (BCL), Botswana," *Journal of Environmental Chemistry and Ecotoxicology*, vol. 8, no. 8, pp. 73–81, Aug. 2016, doi: 10.5897/jece2013.0306.

[3] M. Rosas-Ramírez et al., "Phytoremediation potential of heavy metals using biochar and accumulator plants: A sustainable approach towards cleaner environments," *Plants*, vol. 14, no. 22, art. no. 3470, Nov. 2025, doi: 10.3390/plants14223470.

[4] L. Wang, B. Ji, Y. Hu, R. Liu, and W. Sun, "A review on in situ phytoremediation of mine tailings," *Chemosphere*, vol. 184, pp. 594–600, Oct. 2017, doi: 10.1016/j.chemosphere.2017.06.025.

[5] B. Nedjimi, "Phytoremediation: a sustainable environmental technology for heavy metals decontamination," *SN Applied Sciences*, vol. 3, no. 3, art. no. 286, Feb. 2021, doi: 10.1007/s42452-021-04301-4.

[6] L. Saha, J. Tiwari, K. Bauddh, and Y. Ma, "Recent developments in microbe–plant-based bioremediation for tackling heavy metal-polluted soils," *Frontiers in Microbiology*, vol. 12, art. no. 731723, Oct. 2021, doi: 10.3389/fmicb.2021.731723.

[7] T. Manyiwa et al., "Heavy metals in soil, plants, and associated risk on grazing ruminants in the vicinity of Cu–Ni mine in Selebi-Phikwe, Botswana," *Environmental Geochemistry and Health*, vol. 44, no. 5, pp. 1633–1648, May 2022, doi: 10.1007/s10653-021-00918-x.

[8] P. R. Yaashikaa, P. S. Kumar, S. Varjani, and A. Saravanan, "A critical review on the biochar production techniques, characterization, stability and applications for circular bioeconomy," *Biotechnology Reports*, vol. 28, art. no. e00570, Dec. 2020, doi: 10.1016/j.btre.2020.e00570.

[9] M. Ahmad et al., "Biochar as a sorbent for contaminant management in soil and water: A review," *Chemosphere*, vol. 99, pp. 19–33, Mar. 2014, doi: 10.1016/j.chemosphere.2013.10.071.

[10] E. N. Bakatula, D. Richard, C. M. Neculita, and G. J. Zagury, "Determination of point of zero charge of natural organic materials," *Environmental Science and Pollution Research*, vol. 25, no. 8, pp. 7823–7833, Mar. 2018, doi: 10.1007/s11356-017-1115-7.

[11] A. I. Abd-Elhamid et al., "Enhanced removal of cationic dye by eco-friendly activated biochar derived from rice straw," *Applied Water Science*, vol. 10, no. 1, art. no. 43, Jan. 2020, doi: 10.1007/s13201-019-1128-0.

[12] Z. A. Zahara, I. Royani, N. R. Palapa, R. Mohadi, and A. Lesbani, "Treatment of methylene blue using Ni-Al/magnetite biochar layered double hydroxides composite by adsorption," *Bulletin of Chemical Reaction Engineering & Catalysis*, vol. 18, no. 4, pp. 659–674, Dec. 2023, doi: 10.9767/bcrec.20049.

[13] L. Largitte and R. Pasquier, "A review of the kinetics adsorption models and their application to the adsorption of lead by an activated carbon," *Chemical Engineering Research and Design*, vol. 109, pp. 495–504, May 2016, doi: 10.1016/j.cherd.2016.02.006.

[14] L. Sellaoui, S. Knani, A. Erto, M. A. Hachicha, and A. Ben Lamine, "Equilibrium isotherm simulation of tetrachlorethylene on activated carbon using the double layer model with two energies: Steric and energetic interpretations," *Fluid Phase Equilibria*, vol. 408, pp. 259–264, Jan. 2016, doi: 10.1016/j.fluid.2015.09.022.

[15] N. F. Al-Harby, E. F. Albahly, and N. A. Mohamed, "Kinetics, isotherm and thermodynamic studies for efficient adsorption of congo red dye from aqueous solution onto novel cyanoguanidine-modified chitosan adsorbent," *Polymers*, vol. 13, no. 24, art. no. 4446, Dec. 2021, doi: 10.3390/polym13244446.

[16] A. Y. Al Haj Ahmed, H. Al Najar, and N. A. Ghalwa, "Boron adsorption from aqueous solutions using chemically activated kaolin clay adsorbents kinetics isotherm and thermodynamic studies," *Scientific Reports*, vol. 15, no. 1, art. no. 26758, Jan. 2025, doi: 10.1038/s41598-025-26758-8.

[17] K. Jedynak and B. Charmas, "Adsorption properties of biochars obtained by KOH activation," *Adsorption*, vol. 30, no. 2, pp. 167–183, Feb. 2024, doi: 10.1007/s10450-023-00399-7.

[18] T. Wang, X. Quan, Z. Sun, and Z. Sun, "Sustainable biochar synthesis via synergistic H2O2-KOH modification for enhanced CO2 physisorption," *Carbon Capture Science and Technology*, vol. 15, art. no. 100438, Jun. 2025, doi: 10.1016/j.ccst.2025.100438.

[19] W. H. Xie, X. Yao, H. Li, H. R. Li, and L. N. He, "Biomass-based N-rich porous carbon materials for CO2 capture and in-situ conversion," *ChemSusChem*, vol. 15, no. 18, art. no. e202201004, Sep. 2022, doi: 10.1002/cssc.202201004.

[20] G. Murtaza et al., "Recent trends and economic significance of modified/functionalized biochars for remediation of environmental pollutants," *Scientific Reports*, vol. 14, no. 1, art. no. 1231, Jan. 2024, doi: 10.1038/s41598-023-50623-1.

[21] K. Liepins et al., "Enhancing the wetting properties of activated biochar by oxidation with hydrogen peroxide," *Chemistry (Switzerland)*, vol. 6, no. 5, art. no. 53, Oct. 2024, doi: 10.3390/chemistry6050053.

[22] M. Gale, T. Nguyen, M. Moreno, and K. L. Gilliard-Abdulaziz, "Physiochemical properties of biochar and activated carbon from biomass residue: Influence of process conditions to adsorbent properties," *ACS Omega*, vol. 6, no. 15, pp. 10224–10233, Apr. 2021, doi: 10.1021/acsomega.1c00530.

[23] S. K. Shahcheragh, M. M. Bagheri Mohagheghi, and A. Shirpay, "Effect of physical and chemical activation methods on the structure, optical absorbance, band gap and urbach energy of porous activated carbon," *SN Applied Sciences*, vol. 5, no. 12, art. no. 317, Nov. 2023, doi: 10.1007/s42452-023-05559-6.

[24] T. Prakoso *et al.*, "The Study of Hydrothermal Carbonization and Activation Factors' Effect on Mesoporous Activated Carbon Production From Sargassum sp. Using a Multilevel Factorial Design," *Reaktor*, vol. 22, no. 2, pp. 59–69, Dec. 2022, doi: 10.14710/reaktor.22.2.59-69.

[25] N. A. M. Barakat, M. S. Mahmoud, and H. M. Moustafa, "Comparing specific capacitance in rice husk-derived activated carbon through phosphoric acid and potassium hydroxide activation order variations," *Scientific Reports*, vol. 14, no. 1, art. no. 49675, Jan. 2024, doi: 10.1038/s41598-023-49675-0.

[26] A. M. Dehkhoda, E. Gyenge, and N. Ellis, "A novel method to tailor the porous structure of KOH-activated biochar and its application in capacitive deionization and energy storage," *Biomass and Bioenergy*, vol. 87, pp. 107–121, Apr. 2016, doi: 10.1016/j.biombioe.2016.02.023.

[27] A. Gezahegn et al., "Pyrolysis temperature changes the physicochemical characteristics of water hyacinth-based biochar as a potential soil amendment," *Biomass Conversion and Biorefinery*, vol. 15, no. 3, pp. 3737–3752, Feb. 2025, doi:10.1007/s13399-024-05338-2.

[28] H. Chaudhary, J. Dinakaran, T. Notup, K. Vikram, and K. S. Rao, "Comparison of adsorption performance of biochar derived from urban biowaste materials for removal of heavy metals," *Environmental Management*, vol. 73, no. 2, pp. 408–424, Feb. 2024, doi: 10.1007/s00267-023-01866-1.

[29] M. Rehali, N. El Ghachtouli, S. F. Lange, and R. Bouamri, "Valorization of date palm residues for biochar production: Assessing biochar characteristics for agricultural application," *Scientific African*, vol. 27, art. no. e02599, Mar. 2025, doi: 10.1016/j.sciaf.2025.e02599.

[30] B. D. Zdravkov, J. J. Čermák, M. Šefara, and J. Janků, "Pore classification in the characterization of porous materials: A perspective," *Central European Journal of Chemistry*, vol. 5, no. 2, pp. 385–395, Jun. 2007, doi: 10.2478/s11532-007-0017-9.

[31] M. Thommes et al., "Physisorption of gases, with special reference to the evaluation of surface area and pore size distribution (IUPAC Technical Report)," *Pure and Applied Chemistry*, vol. 87, no. 9–10, pp. 1051–1069, Sep. 2015, doi: 10.1515/pac-2014-1117.

[32] T. I. Ojonimi, F. Asuke, M. A. Onimisi, and C. Y. Onuh, "Acid Mine Drainage (AMD): an environmental concern generated by coal mining," *Journal of Degraded and Mining Lands Management*, vol. 6, no. 4, pp. 1875–1881, Jul.

2019, doi: 10.15243/jdmlm.2019.064.1875.

[33] S. A. Bhat et al., "Phytoremediation of heavy metals in soil and water: An eco-friendly, sustainable and multidisciplinary approach," *Chemosphere*, vol. 303, pt. 2, art. no. 134788, Sep. 2022, doi: 10.1016/j.chemosphere.2022.134788.

[34] E. Hubert and C. Wolkersdorfer, "Establishing a conversion factor between electrical conductivity and total dissolved solids in South African mine waters," *Water SA*, vol. 41, no. 4, pp. 490–500, Jul. 2015, doi: 10.4314/wsa.v41i4.08.

[35] V. M. Ngole-Jeme and J. Ndava, "The implications of AMD induced acidity, high metal concentrations and ochre precipitation on aquatic organisms," *Polish Journal of Environmental Studies*, vol. 32, no. 4, pp. 2959–2980, Jul. 2023, doi: 10.15244/pjoes/161323.

[36] S. Chellappan, V. Nair, V. Sajith, and K. Aparna, "Synthesis, optimization and characterization of biochar based catalyst from sawdust for simultaneous esterification and transesterification," *Chinese Journal of Chemical Engineering*, vol. 26, no. 12, pp. 2654–2663, Dec. 2018, doi: 10.1016/j.cjche.2018.02.034.

[37] R. Vurayai, B. Nkoane, B. Moseki, and P. Chaturvedi, "Assessment of heavy metal pollution/contamination in soils east and west of the Bamangwato Concessions Ltd (BCL) Cu/Ni mine smelter in Selebi-Phikwe, Botswana," *Journal of Biodiversity and Environmental Sciences*, vol. 7, no. 6, pp. 111–120, Dec. 2015, [Online]. Available: http://www.innspub.net

[38] G. Ishmael, V. U. Ultra, G. Rantong, O. A. Keitshweditse, and K. L. Sefatlhi, "Heavy metal accumulation of aquatic grasses from mine tailing's wastewater drainage spillway of BCL Cu-Ni mine in Selebi Phikwe, Botswana," *Environmental Quality Management*, vol. 34, no. 2, pp. 1–17, Dec. 2024, doi: 10.1002/tqem.22271.

[39] M. Saa-Aondo et al., "Efficiencies of heavy metal hyper-accumulation plants as potential land remediators for heavy metal polluted soils," *Asian Journal of Current Research*, vol. 9, no. 1, pp. 60–70, Feb. 2024, doi: 10.56557/ajocr/2024/v9i18525.

[40] N. Arveti, K. S. Kumar, and P. J. C. Favas, "Phytoremediation potential of native plant species for heavy metal contamination in the abandoned Kolar gold fields, Karnataka, South India," *Discover Geoscience*, vol. 3, art. no. 200, Feb. 2025, doi: 10.1007/s44288-025-00318-z.

[41] R. Huang, B. Zhang, E. M. Saad, E. D. Ingall, and Y. Tang, "Speciation evolution of zinc and copper during pyrolysis and hydrothermal carbonization treatments of sewage sludges," *Water Research*, vol. 132, pp. 260–269, Apr. 2018, doi: 10.1016/j.watres.2018.01.009.

[42] E. M. C. C. Batista et al., "Effect of surface and porosity of biochar on water holding capacity aiming indirectly at preservation of the Amazon biome," *Scientific Reports*, vol. 8, art. no. 10677, Jul. 2018, doi: 10.1038/s41598-018-28794-z.

[43] J. A. Ippolito, T. F. Ducey, K. A. Spokas, K. M. Trippe, and M. G. Johnson, "A biochar selection method for remediating heavy metal contaminated mine tailings," *International Journal of Environmental Science and Technology*, vol. 21, no. 15, pp. 9611–9622, Dec. 2024, doi: 10.1007/s13762-024-05621-9.

[44] E. Sørmo et al., "Heavy metals in pyrolysis of contaminated wastes: Phase distribution and leaching behaviour," *Environments*, vol. 11, no. 6, art. no. 130, Jun. 2024, doi: 10.3390/environments11060130.

[45] J. Doble, G. Wilson, and J. W. Wainman, "Kinetic and thermodynamic analysis of the adsorption of methylene blue onto biochar," *Journal of Chemical Education*, vol. 100, no. 10, pp. 4040–4046, Oct. 2023, doi: 10.1021/acs.jchemed.3c00518.

[46] H. Lee, S. Fiore, and F. Berruti, "Adsorption of methyl orange and methylene blue on activated biocarbon derived from birchwood pellets," *Biomass and Bioenergy*, vol. 191, art. no. 107446, Dec. 2024, doi: 10.1016/j.biombioe.2024.107446.

[47] N. Vasiljević, S. Panić, G. Tadić, J. Vuković, N. Novaković, and V. Mićić, "Investigation of the kinetics of the adsorption of methylene blue on activated carbon," *Engineering Proceedings*, vol. 99, no. 1, art. no. 4, Feb. 2025, doi: 10.3390/engproc2025099004.

[48] M. A. O. Y. Weeratunge, M. D. N. Dinusha, R. M. M. K. Karunathilaka, and N. Priyantha, "Comparative adsorption characteristics of methylene blue on raw leaves and biochar of guinea grass (Megathyrsus maximus)," *Discover Chemistry*, vol. 3, art. no. 50, Feb. 2026, doi: 10.1007/s44371-026-00496-w.

[49] P. S. Kumar, S. Ramalingam, and K. Sathishkumar, "Removal of methylene blue dye from aqueous solution by activated carbon

prepared from cashew nut shell as a new low-cost adsorbent," *Korean Journal of Chemical Engineering*, vol. 28, no. 1, pp. 149–155, Jan. 2011, doi: 10.1007/s11814-010-0342-0.

[50] E. Duque-Brito, D. R. Lobato-Peralta, J. A. Okolie, D. M. Arias, P. J. Sebastian, and P. U. Okoye, "Fast-kinetics adsorption of a binary solution containing cationic and ionic pollutants using high-surface area activated carbon derived from macadamia nutshell," *Energy, Ecology and Environment*, vol. 9, no. 1, pp. 84–99, Feb. 2024, doi: 10.1007/s40974-023-00304-6.

[51] A. F. Alshekhli, H. A. Hasan, M. H. Muhamad, and S. R. Sheikh Abdullah, "Development of adsorbent from phytoremediation plant waste for methylene blue removal," *Journal of Ecological Engineering*, vol. 21, no. 8, pp. 207–215, Nov. 2020, doi: 10.12911/22998993/126873.

[52] A. A. Basaleh, M. H. Al-Malack, and T. A. Saleh, "Methylene Blue removal using polyamide-vermiculite nanocomposites: Kinetics, equilibrium and thermodynamic study," *Journal of Environmental Chemical Engineering*, vol. 7, no. 3, art. no. 103107, Jun. 2019, doi: 10.1016/j.jece.2019.103107.

[53] Z. Liu, M. Azharul Islam, and J. Huang, "Study of the adsorption of methylene blue by phytoremediation-plant biomass carbon," *Journal of Molecular Liquids*, vol. 366, art. no. 120273, Nov. 2022, doi: 10.1016/j.molliq.2022.120273.

[54] O. S. Olugbenga, P. G. Adeleye, S. B. Oladipupo, A. T. Adeleye, and K. I. John, "Biomass-derived biochar in wastewater treatment- a circular economy approach," *Waste Management Bulletin*, vol. 1, no. 4, pp. 1–14, Jan. 2024, doi: 10.1016/j.wmb.2023.07.007.

[55] N. S. Pham et al., "Adsorption of orange G using activated carbon derived from common reed (Phragmites australis) in Mekong Delta, Vietnam," *Desalination and Water Treatment*, vol. 317, art. no. 100095, Mar. 2024, doi: 10.1016/j.dwt.2024.100095.

[56] Z. Bu, Y. Fang, H. Chen, M. Zhang, and F. Wang, "Study on the adsorption properties of organically modified diatomite for methylene blue," *Scientific Reports*, vol. 15, art. no. 13768, Jan. 2025, doi: 10.1038/s41598-025-13768-9.

[57] M. A. Islam, A. Benhouria, M. Asif, and B. H. Hameed, "Methylene blue adsorption on factory-rejected tea activated carbon prepared by conjunction of hydrothermal carbonization and sodium hydroxide activation processes," *Journal of the Taiwan Institute of Chemical Engineers*, vol. 52, pp. 57–64, Jul. 2015, doi: 10.1016/j.jtice.2015.02.010.

[58] N. Mekonen, S. Gebrearegawi, Y. Syraji, and K. Tsegaye, "Low cost adsorbent derived from agricultural byproduct and its application for the removal of cationic dye from waste water: A review," *American Journal of Biological and Environmental Statistics*, vol. 10, no. 3, pp. 67–75, Sep. 2024, doi: 10.11648/j.ajbes.20241003.14.

[59] L. Ton-That et al., "Kinetic studies of the removal of methylene blue from aqueous solution by biochar derived from jackfruit peel," *Environmental Monitoring and Assessment*, vol. 195, no. 11, art. no. 1266, Oct. 2023, doi: 10.1007/s10661-023-11867-6.

[60] F. C. Wu, R. L. Tseng, and R. S. Juang, "Characteristics of Elovich equation used for the analysis of adsorption kinetics in dye-chitosan systems," *Chemical Engineering Journal*, vol. 150, no. 2–3, pp. 366–373, Aug. 2009, doi: 10.1016/j.cej.2009.01.014.

[61] C. H. C. Tan, S. Sabar, and M. H. Hussin, "Development of immobilized microcrystalline cellulose as an effective adsorbent for methylene blue dye removal," *South African Journal of Chemical Engineering*, vol. 26, pp. 11–24, Oct. 2018, doi: 10.1016/j.sajce.2018.08.001.

[62] J. Ghasemi and S. Asadpour, "Thermodynamics' study of the adsorption process of methylene blue on activated carbon at different ionic strengths," *Journal of Chemical Thermodynamics*, vol. 39, no. 6, pp. 967–971, Jun. 2007, doi: 10.1016/j.jct.2006.10.018.

[63] V. J. Inglezakis and A. A. Zorpas, "Heat of adsorption, adsorption energy and activation energy in adsorption and ion exchange systems," *Desalination and Water Treatment*, vol. 39, no. 1–3, pp. 149–157, Feb. 2012, doi: 10.5004/dwt.2012.3000.

[64] S. Mabrouk and H. Dhaouadi, "Experimental study and theoretical modelling based on DFT of the elimination of ceftriaxone by an activated carbon synthesized from grape seeds waste," *Scientific Reports*, vol. 15, art. no. 27184, Feb. 2025, doi: 10.1038/s41598-025-27184-6.

[65] S. Satyam and S. Patra, "Innovations and challenges in adsorption-based wastewater remediation: A comprehensive review," *Heliyon*, vol. 10, no. 9, art. no. e29573, May

2024, doi: 10.1016/j.heliyon.2024.e29573.

[66] W. H. Lee, J. S. Park, J. H. Sok, and P. J. Reucroft, "Effects of pore structure and surface state on the adsorption properties of nano-porous carbon materials in low and high relative pressures," *Applied Surface Science*, vol. 246, no. 1–3, pp. 77–81, Jun. 2005, doi: 10.1016/j.apsusc.2004.10.038.

[67] J. Wang, Y. Tan, H. Yang, L. Zhan, G. Sun, and L. Luo, "On the adsorption characteristics and mechanism of methylene blue by ball mill modified biochar," *Scientific Reports*, vol. 13, art. no. 21085, Nov. 2023, doi: 10.1038/s41598-023-48373-1.

[68] S. Sahu *et al.*, "Adsorption of methylene blue on chemically modified lychee seed biochar: Dynamic, equilibrium, and thermodynamic study," *Journal of Molecular Liquids*, vol. 315, art. no. 113743, Oct. 2020, doi: 10.1016/j.molliq.2020.113743..

[69] S. P. Viswanthan *et al.*, "Removal efficiency of methylene blue from aqueous medium using biochar derived from Phragmites karka, a highly invasive wetland weed," *Biomass Conversion and Biorefinery*, vol. 12, no. 8, pp. 3257–3273, Aug. 2022, doi: 10.1007/s13399-020-00877-w.